

Electron irradiation on multilayer $PdSe_2$ field effect transistors

A. Di Bartolomeo^{1,2,a)}, F. Urban^{1,2,3}, A. Pelella^{1,2}, A. Grillo^{1,2}, M. Passacantando⁴, X. Liu⁵ and F. Giubileo²

¹*Department of Physics, University of Salerno, via Giovanni Paolo II, Fisciano, 84084, Italy*

²*CNR-SPIN, via Giovanni Paolo II, Fisciano, 84084, Italy*

³*INFN – Gruppo collegato di Salerno, via Giovanni Paolo II, Fisciano, 84084, Italy*

⁴*Department of Physical and Chemical Sciences, University of L'Aquila, and CNR-SPIN L'Aquila, via Vetoio, Coppito 67100, Italy*

⁵*National Laboratory of Solid State Microstructures, School of Physics, Collaborative Innovation Center of Advanced Microstructures, Nanjing University, Nanjing, 210093, China*

^{a)}*Author to whom correspondence should be addressed. Electronic mail: adibartolomeo@unisa.it.*

Abstract

Palladium diselenide ($PdSe_2$) is a recently isolated layered material that has attracted a lot of interest for the pentagonal structure, the air stability and the electrical properties largely tunable by the number of layers. In this work, $PdSe_2$ is used in the form of multilayer as the channel of back-gate field-effect transistors, which are studied under repeated electron irradiations. Source-drain Pd leads enable contacts with resistance below $350\text{ k}\Omega \cdot \mu\text{m}$. The transistors exhibit a prevailing n-type conduction in high vacuum, which reversibly turns into ambipolar electric transport at atmospheric pressure. Irradiation by 10 keV electrons suppresses the channel conductance and promptly transforms the device from n-type to p-type. An electron fluence as low as $160\text{ e}^-/\text{nm}^2$ dramatically change the transistor behavior demonstrating a high sensitivity of $PdSe_2$ to electron irradiation. The sensitivity is lost after few exposures, that is a saturation condition is reached for fluence higher than $\sim 4000\text{ e}^-/\text{nm}^2$. The damage induced by high electron fluence is irreversible as the device persist in the radiation-modified state for several hours, if kept in vacuum and at room temperature. With the support of numerical simulation, we explain such a behavior by electron-induced Se atom vacancy formation and charge trapping in slow trap states at the Si/SiO_2 interface.

^{a)} Author to whom correspondence should be addressed. Electronic mail: adibartolomeo@unisa.it.

Introduction

Two dimensional materials such as graphene^{1,2} and transition-metal dichalcogenides³ (TMDs) have been considered for several applications and in particular for space instrumentation⁴ due to their low size and weight, the high robustness and chemical inertness, and the unique optoelectronic properties⁵⁻⁸. The use in space electronics, sensors, batteries, photovoltaics or light sources requires qualifications against vibrations and shocks, vacuum and thermal cycles, and exposure to radiation. In general, vibrations and shocks are not a threat for nanodevices and vacuum and thermal cycles are widely experimented in laboratories⁹⁻¹². Similarly, the effect of radiation has been largely investigated for graphene¹³⁻¹⁶ and well-known TMDs, such as MoS_2 , WS_2 , $MoSe_2$, and WSe_2 ^{13,17-22}, although most of the irradiation studies have been carried out using high energy protons, ions, electrons or γ beams, typically in the MeV range. However, the application of these materials in the context of radiation-based medical diagnostics and treatments, radioprotection, monitoring of special nuclear materials or instrumentation, and in other areas of nuclear science, also requires the understanding of their behavior when exposed to lower energy radiation sources. Low-energy ($<100\text{ keV}$) electron beams are commonly used during device fabrication by electron beam lithography (EBL) as well as for characterization and imaging through scanning and transmission electron microscopy (SEM and TEM). Exposure to low energy electrons also occurs in plasma treatments often used for device fabrication.

While high energy charged particles have reduced probability of interaction in few-layer materials and primarily damage the supporting substrate, low-energy electrons can produce significant modifications of the properties of 2D-materials based devices. Their stopping power in 2D materials becomes higher at decreasing energies below 100 keV ^{4,23}. Elastic and inelastic scattering of low energy electrons can cause ionization and atomic displacement or sputtering, creating interstitials and vacancies, which impact the electronic performance of graphene or TMDs. Indeed, using first-principles simulations, it has been calculated that the displacement threshold energies and the formation energies of chalcogen vacancies lays between 4 and 8 eV in most common TMDs^{21,24}. The maximum energy transferred by 80 keV electrons to a S (or Mo) atom in MoS_2 is 6 (or 2) eV ²⁵, and the formation of vacancies due to S sputtering in MoS_2 sheets has been demonstrated by TEM under 80 keV electron beam irradiation²⁴. It has been also shown that the filling of the such vacancies with impurity atoms can control the doping of the material, thereby suggesting new ways for engineering the

electronic structure of TMDs²⁶. Analogously, the formation of vacancies due to Se sputtering in WSe_2 create localized carrier-trapping deep states within the band gap and, if two adjacent Se atoms are removed in the same chalcogenide layer, the change in the local crystal structure induces a transition from direct to indirect band gap²³. It has been also reported that 1 keV to 3 keV electron irradiation can transform the structure of the MoS_2 films from amorphous to crystalline, thus enhancing the performance of MoS_2 - based photodetectors²⁷. The capability of electron-beam irradiation to generating vacancies has enabled patterning and cutting of graphene or MoS_2 in nanoribbons^{25,28,29}. Using SEM electron beams at energies 5, 10, 20 and 30 keV, it has been found that high electron fluences ($\sim 10^4 e^-/nm^2$) result in permanent loss of photoluminescence for WS_2 monolayers, owing to the creation of chalcogen vacancies by knock-on damage, which cause recombination and quenching of the photoluminescence⁴. Remarkably, even at the highest fluences, the radiation induced damage was found to be mitigated if the electron energy increased to 30 keV as higher-energy electrons have a smaller interaction cross-section.

In this paper, we investigate the properties of multilayer $PdSe_2$ that we use as the channel of back-gate field effect transistors. $PdSe_2$ is a noble-metal TMD with pentagonal structure and puckered layers, which is air stable³⁰⁻³². It has been obtained in the 2D form only recently³⁰ and is still poorly understood, even though it has been already exploited for high-sensitivity photodetectors^{33,34}, field effect transistors^{9,35}, thermoelectric devices³⁶, field emitter³⁷ or water splitting³⁸. The choice of nanosheets consisting of several layers is motivated by the recent discovery that defects in $PdSe_2$ can induce strong interlayer interactions and lead to the formation of new material phases. Indeed, it has been reported that the formation of Se vacancies by 60 keV electron irradiation in $PdSe_2$ can lead to local interlayer melding and result in the formation of the new Pd_2Se_3 2D phase³⁹. Here, we show that the use of Pd leads over multilayer $PdSe_2$ nanosheets give rise to contacts with relatively low resistance even without any special treatments. We demonstrate that the dominant n-type conduction in high vacuum can be turned into an ambipolar or p-type one either by raising the pressure in air or by electron irradiation. We demonstrate that long exposure to 10 keV electron beam in a SEM chamber changes the channel doping and transform the device from n- to p-type. Using Monte Carlo simulations, we show that the electron beam induces defects mainly in the $PdSe_2$ nanosheet and at the interface between the Si back-gate and the SiO_2 gate dielectric. Such defects permanently change the electric conduction in the

device. This study highlights a high sensitivity of $PdSe_2$ to low-energy electron irradiation, a finding that limits its use in radiation-rich environments and requires caution when an electron beam is used for device fabrication and analysis, but could enable high-sensitive radiation detectors for application in medical or nuclear instrumentation, radioprotection and radiotherapy and environmental monitoring.

Fabrication and methods

$PdSe_2$ nanosheets were exfoliated from bulk $PdSe_2$ single-crystal by the adhesive tape method and transferred onto a highly-doped p-type silicon substrate covered with 300 nm thick SiO_2 . The $PdSe_2$ single-crystal was synthesized through a two-step thermal process from compressed tablets of selenium (99.999 %) and palladium (99.95 %) powders, mixed in the atomic ratio of 2: 1. The tablets were heated up at 850 °C for 72 h in a quartz tube at 10^{-5} mbar pressure. Finally, the cooled down poly-crystalline $PdSe_2$ tablets were mixed with Se powder in a mass ratio of 1: 4 and subjected to a second similar temperature annealing cycle.

The stoichiometric $Pd:Se$ atomic ratio close to 1: 2 and layered crystallographic structure along the c -axis of the transferred nanosheets (the unit cell of $PdSe_2$ is orthorhombic with space group $Pbca$ ^{30,40,41}) were confirmed by energy dispersive X-ray spectroscopy, X-ray diffractometry and Raman spectroscopy as reported in a previous work, where we used the same production batch⁴².

Nanosheets with thickness of 10 – 15 nm were used for device fabrication through electron-beam lithography, metal evaporation and lift-off. Several structures for transfer length measurements (TLM) were contacted using Pd/Au (5/40 nm) leads. An example of a long flake, 2.5 μm wide, with six Pd/Au leads at a distance of 1.5 μm from each other, is shown in Figure 1(a). The z -profile, obtained by atomic-force microscope (AFM), shows that the nanosheet has a thickness of 12 nm (Figure 1(b) and 1(c)) corresponding to ~30 atomic layers (the theoretical thickness of a monolayer is 0.41 nm³⁵).

The electrical characterization of the device was carried out by means of a Keithley 4200 semiconductor analyzer in three-terminal configuration, as shown in schematic setup of Figure 1(d), where two top metal leads are the source and drain and the silicon substrate is the back gate of a field effect transistor. The electrical measurements were performed inside a scanning electron microscope (SEM) chamber (ZEISS, LEO 1530) at room temperature and, if not otherwise specified, at pressure $\sim 10^{-6}$ torr. The 10 keV and 10 pA electron beam of the SEM was used for time-controlled irradiations of the channel region.

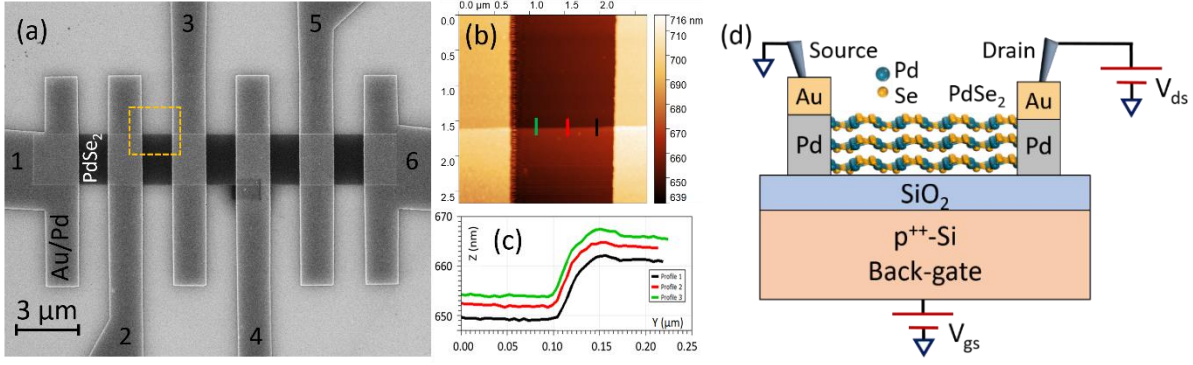


Figure 1: SEM image of a $PdSe_2$ nanosheet contacted with Pd/Au leads. AFM image (b) and step height profile (c) of the $PdSe_2$ nanosheet. (d) Layout of the $PdSe_2$ field-effect transistor and biasing of the back-gate transistor in common-source configuration.

Results and discussion

Figure 2 (a) shows the common-source transfer characteristics (drain-current versus gate-voltage, $I_{ds} - V_{gs}$, at fixed drain-voltage, V_{ds}) of the transistor between metal leads labelled 5 and 6, at different pressures. The device, kept at $\sim 10^{-6}$ Torr for several hours, shows electron dominant conduction over the ± 50 V range (larger biases were avoided to prevent dielectric damage). The transistor has on/off ratio around 50, a negative threshold voltage, $V_{th} \sim -10$ V, and a maximum field-effect electron mobility $\mu = \frac{L}{W} \frac{1}{C_{SiO_2}} \frac{1}{V_{ds}} \frac{dI_{ds}}{dV_{gs}} \sim 30 \text{ cm}^2 V^{-1} s^{-1}$ ($C_{SiO_2} = 11 \text{ nF cm}^{-2}$ is the capacitance per unit area of the 300 nm SiO_2 gate dielectric, $L = 1.5 \mu m$ and $W = 2.5 \mu m$ are the channel length and width, respectively). The electron mobility is within the range reported for similar ultrathin $PdSe_2$ devices^{30,33,35,43}.

The low-bias output characteristics ($I_{ds} - V_{ds}$ curves at given V_{gs}) are straight-lines and the back-gate modulates the channel current without changing the linearity, as shown in Figure 2(b).

The n-type behavior of the transistor and the linear output curves can be understood considering a low intrinsic n-type doping of $PdSe_2$ and an ideal band alignment with the Pd metal contacts⁴⁴⁻⁴⁶. The intrinsic n-type doping can be caused by intrinsic defects such as selenium vacancies⁴⁷⁻⁴⁹. The presence of defects in the $PdSe_2$ channel is strongly suggested by the clockwise hysteresis obtained when the gate voltage is swept back and forth⁵⁰⁻⁵². Furthermore, the work function difference between the 12 nm thick $PdSe_2$ (work function $\sim 5.0 \text{ eV}$ ⁴⁷) and the Pd contacts (work function $\geq 5.20 \text{ eV}$ ^{53,54}) originates a band bending that favours the electron conduction, as shown in the schematic energy diagram along the channel direction in the inset of

Figure 2 (b). The low Schottky barriers at the contacts, owed to the small work function difference and the narrow bandgap of $PdSe_2$, that for ~ 30 layers is less than $0.3 eV$ ^{31,33,47}, can contribute to the contact resistance but does not cause rectification at low bias. We note that, differently from here, non-linear output characteristics were reported for $PdSe_2$ with similar channel thickness and Pd/Au contact³³, but this could be ascribed to a slight asymmetry of the two Schottky barriers which seems not to occur in the device under study⁴⁵.

Furthermore, Figure 2(a) shows that the behavior of the transistor is dramatically changed by pressure, as often reported for TMDs materials^{42,43,55–57}. The raising pressure gradually suppresses the channel current and the transistor becomes ambipolar at atmospheric pressure. The effect of pressure has been widely investigated and mainly attributed to adsorption of molecular O_2 and water at defect sites which counter-dope the channel till reverting its polarity^{42,48,52,58}. As shown in Figure 2(a), the effect of pressure is fully reversible as the transistor returns to its pristine status if the high vacuum is restored in a time of few hours⁴⁸.

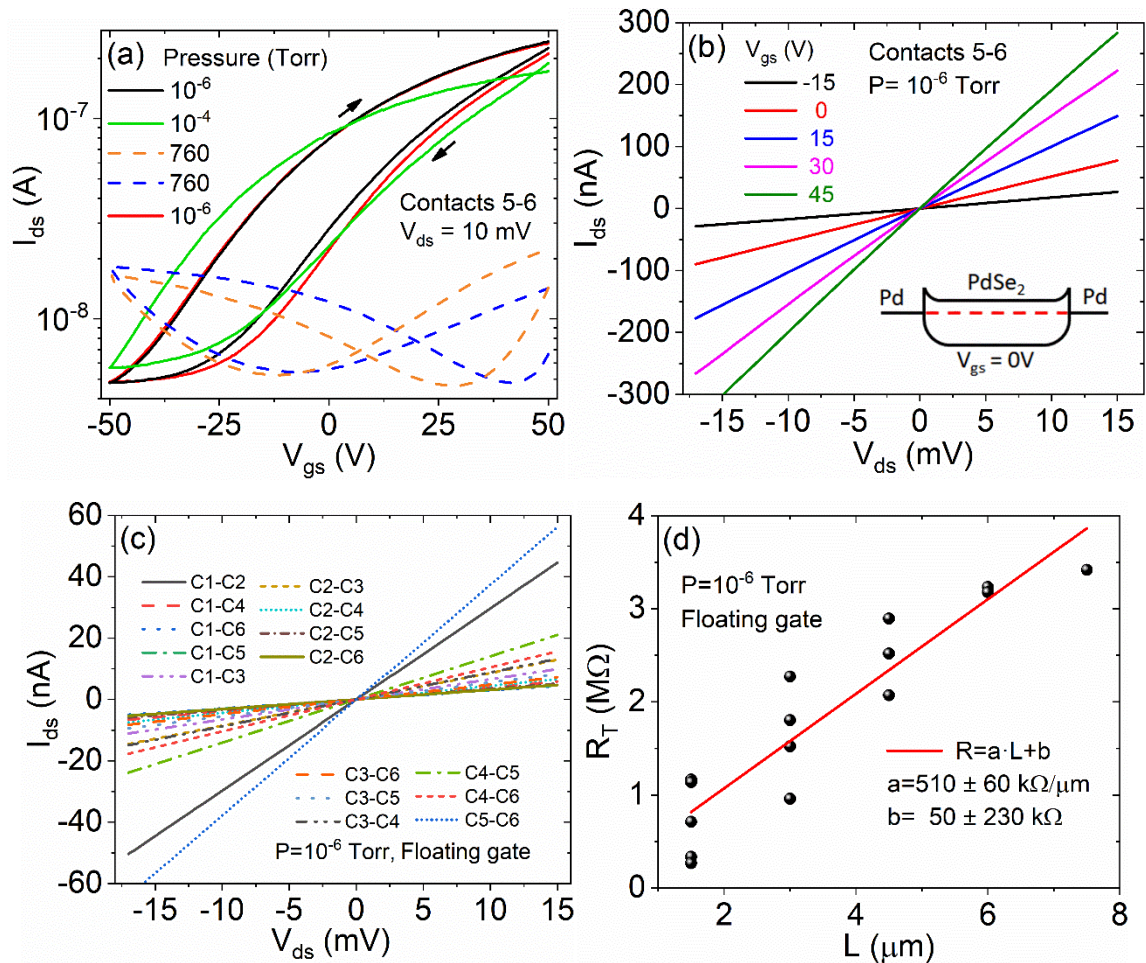


Figure 2: Transfer characteristics at various pressures in time sequence (a) and output characteristics (b) at 10^{-6} Torr of the transistor with $PdSe_2$ channel between leads 5 and 6. The inset of (b) shows the band energy diagram along the channel direction for grounded gate. Output characteristics between different combinations of the metal contacts (c) and external resistance versus channel length (L) at $\sim 10^{-6}$ Torr and for floating gate (the $PdSe_2$ length covered by floating metal leads between source and drain is not included in L).

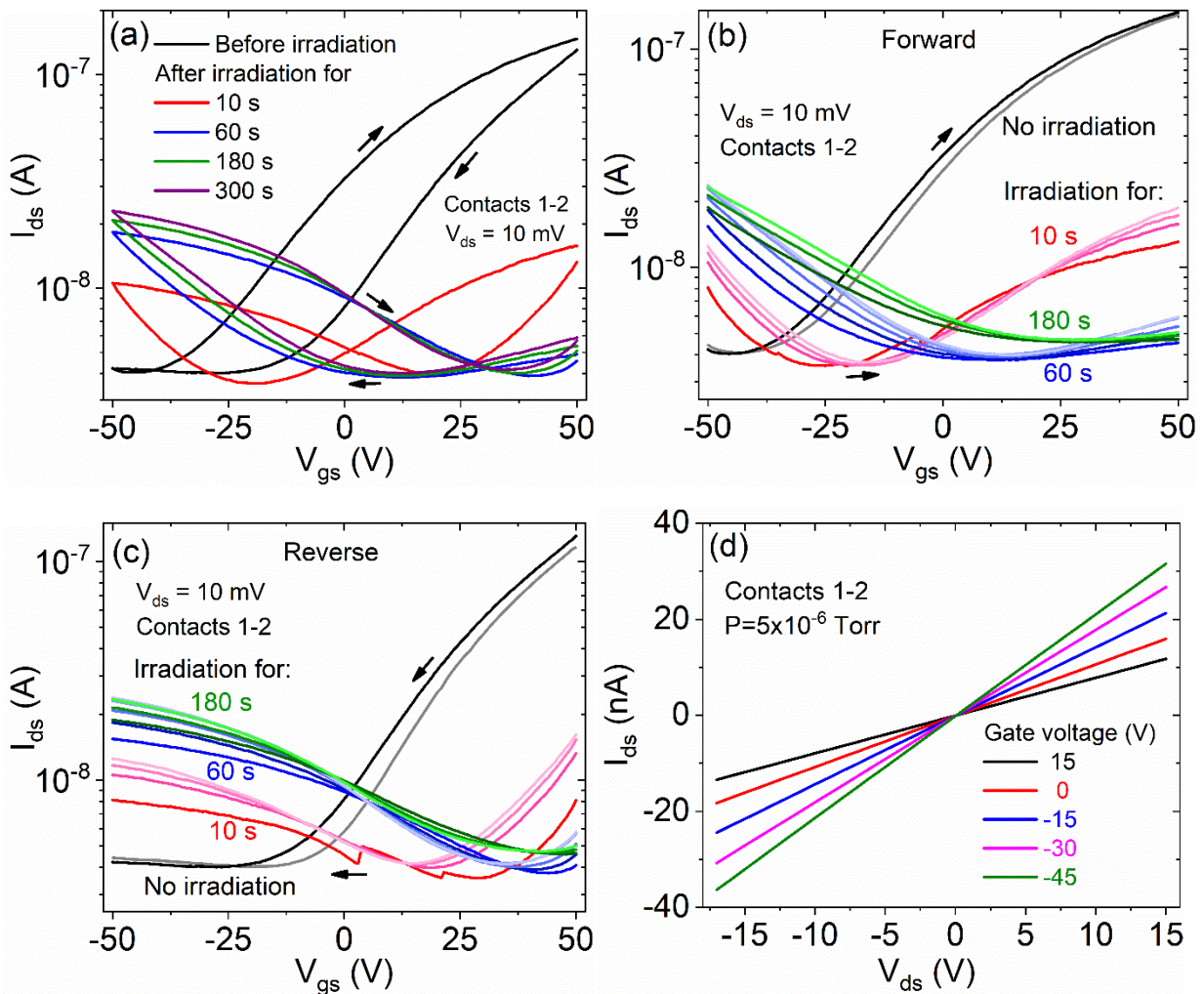
Figure 2(c) displays the output characteristics at floating gate of other devices of the same TLM structure obtained considering different couples of the metal leads; remarkably, the linear behavior is maintained even if the source and drain include one or more floating contacts in between. From Figure 2(c), we extracted the external (source-drain) resistance, R_T , as a function of the channel length, which is shown in Figure 3(d). R_T includes the two contact resistances, R_C , assumed equally distributed between the two contacts, and the channel resistance^{59,60}, $R_{Ch} = R_{Sh} \frac{W}{d}$, where R_{Sh} is the channel sheet resistance in $\frac{\Omega}{square}$ and L is the separation between two leads:

$$R_T = 2R_C + R_{Sh} \frac{L}{W}$$

From the straight line fitting of Figure 3(d), we obtain $R_C = 25 \pm_{-25}^{+120} k\Omega$ and $R_{Sh} = 1.27 \pm 0.15 \frac{M\Omega}{square}$. The contact resistance can be expressed as the specific contact resistance, normalized by the width of the $PdSe_2$ channel, $\rho_c = R_C W = 60 \pm_{-60}^{+300} k\Omega \cdot \mu m$. Despite the high uncertainty, the maximum contact resistance of $360 k\Omega \cdot \mu m$ is significantly lower than the contact resistance $\geq 1 M\Omega \cdot \mu m$ obtained with as-deposited Ti^{35,61} or Ni³¹ contacts, thus confirming the good choice of Pd as for the metal leads. The sheet resistance is comparable to that measured in grain structures of monolayer MoS_2 with missing S⁶² or undoped multilayer MoS_2 (with comparable mobility)⁶³ and even lower than in undoped WSe_2 monolayers⁶⁴.

To study the effect of the irradiation by an electron beam at $10 keV$ and $10 pA$, commonly used for SEM imaging, we selected the device between lead 1-2, which is the second most conducting transistor of the TLM structure according to Figure 2(c). The channel of such transistor had not been exposed to irradiation before, besides that from fast and low magnification imaging of the entire device area, corresponding to very low fluence on the channel region. We characterized the device shortly before and soon after each irradiation by repeatedly measuring the transfer and output characteristics. To control the electron fluence, the irradiation was performed by selecting only the channel region and imaging it for given times. Figure 3(a) shows that electron irradiation has an effect somehow similar to pressure as it suppresses the channel conductance and changes the conduction polarity. The effect of the irradiation is further clarified in Figures 3(b) and 3(c) which show the forward and the reverse branches of the transfer characteristics, respectively. Starting from the

unirradiated device, three distinct groups of transfer characteristics (taken one after the other between consecutive irradiations) can be distinguished, corresponding to successive irradiations of 10 s, 60 s, 180 s (corresponding to total fluences of $165 e^-/nm^2$, $1170 e^-/nm^2$, $4160 e^-/nm^2$). Surprisingly, Figure 3 (a) shows that most of the change occurs already at the low fluence of $165 e^-/nm^2$, i.e. after the first 10 s irradiation, which is enough to significantly suppress the channel conductance and cause the appearance of a p-type conduction. Such an effect is enhanced by the successive 60 s irradiation. Further irradiation of 180 s or more provoke only minor modifications. This observation indicates that the device becomes gradually insensitive to the electron irradiation, meaning that the effect of electron irradiation saturates after a certain fluence. However, while low fluence irradiation can make reversible changes, that might be annealed after 1 h at room temperature, as we have reported before⁹, here we found that a total irradiation time of 550 s set the device in a new state in which it persisted for the observation time of about 5 h.



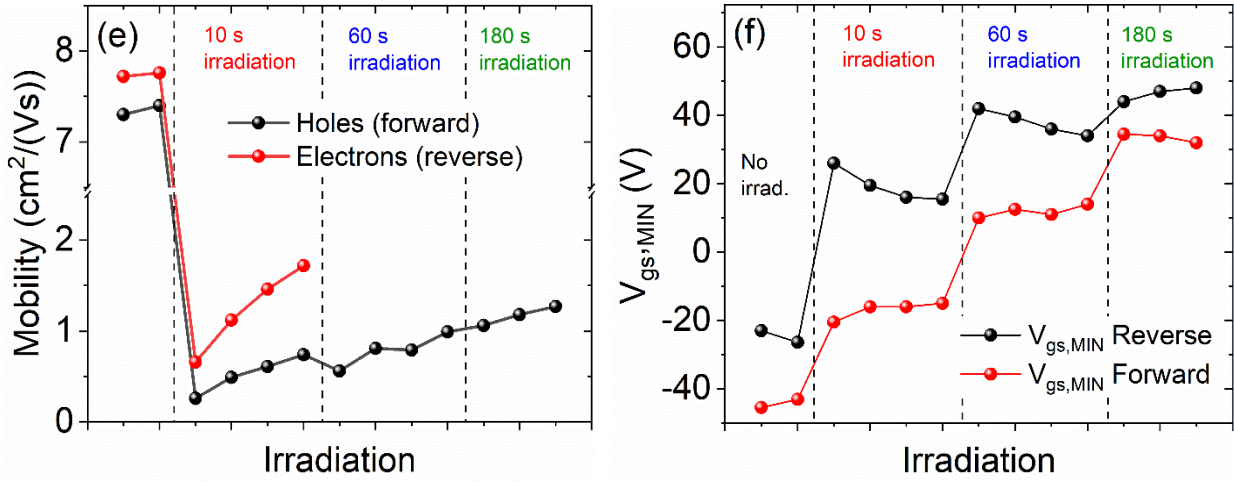


Figure 3: Full-loop (a), forward branch (b) and reverse branch (c) of the transfer characteristics of the transistor between leads 1-2 after electron beam irradiation of different duration. (d) Output characteristics after the whole cycle of irradiations. (e) Field effect mobility as a function of the electron beam irradiation. (f) Effect of the irradiation on conductance minimum, $V_{gs,MIN}$.

Figure 3(d) shows that, despite the decrease of the transistor current, the linear behaviour of the output characteristics is unaffected. The linearity is essentially related to the properties of the $Pd/PdSe_2$ interface, which is preserved as we avoided irradiation of the $Pd/PdSe_2$ contact region. Figures 3(e) and 3(f) demonstrate that the irradiation results in a significant degradation of the charge carrier mobility as well as in a right-shift of the minimum conductance points, $V_{gs,MIN}$, obtained from both the forward and the reverse transfer curves. The mobility degradation is indicative of structural damaging and charge trapping that may generate long range coulomb scattering, while the right-shift corresponds to a doping change as the device gradually becomes p-type.

To further understand the effect of the 10 keV electron beam, we performed Monte Carlo simulation to track the electrons trajectories and the energy loss into the materials. The energy released by electrons can be estimated through the cathodoluminescence, i.e. the light emission caused by electron excitation, whose intensity is shown in Figure 4 (a). We used CASINO software^{65,66}, a Monte Carlo simulator of electron trajectories in solids, specially designed for low-energy beam interaction in bulk and thin foils and widely used in scanning electron microscopy and microanalysis.

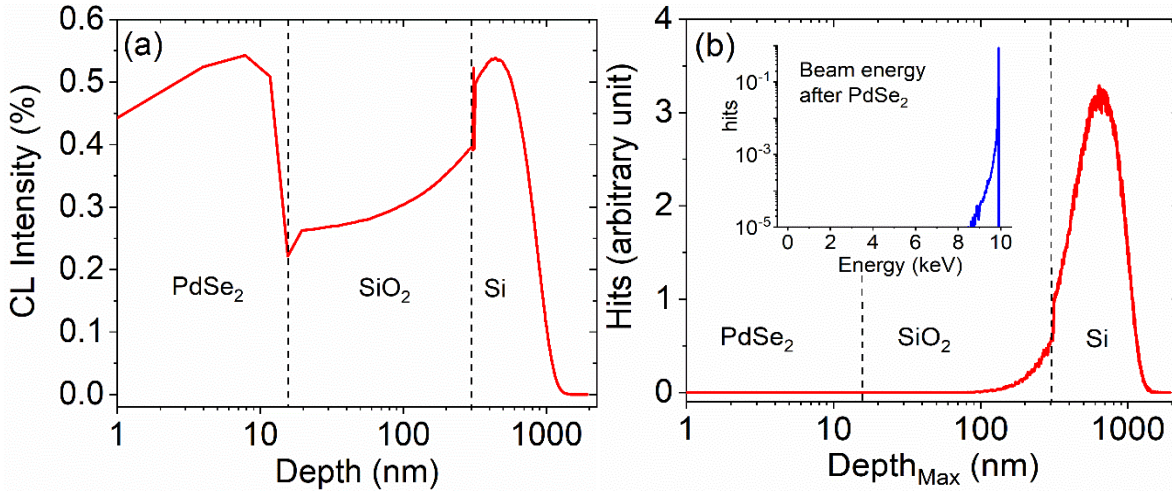


Figure 4: Monte Carlo simulation by CASINO software of the cathodoluminescence intensity (a) and the maximum penetration depth (b), normalized to the total range. The inset of figure (b) shows the transmitted energy when the 10 keV beam emerges from the $PdSe_2$ nanosheet.

The simulation shows that the rate of energy loss in $PdSe_2$ and Si are comparable and higher than in SiO_2 . As expected, most of the energy is released in the silicon substrate where the electrons penetrate for about $\sim 1 \mu m$ as shown by Figure 4(b) reporting the maximum penetration depth. The inset of Figure 4(b) confirms that there is energy loss in the $PdSe_2$ layer. The energy loss in $PdSe_2$ can be up to 2 keV, enough to cause atom displacement or sputtering⁶⁷. The appearance of defects, preferentially Se vacancies as the energy required to displace the chalcogen ($\leq 7 eV$) is about three times lower than that required to remove the transition metal from the same crystal⁶⁷, causes the observed reduction of the charge carrier mobility. Figure 4(a) also shows that there is an uptick in the release of energy at the SiO_2/Si interface. The formation of defects at such interface introduces electron trap states⁶⁸⁻⁷⁰, which can contribute to enhance the p-type doping of the $PdSe_2$ channel. The pile-up of negative charge at the SiO_2/Si during prolonged irradiation exposures acts as an extra negatively-biased gate and right-shift $V_{gs,MIN}$ thus increasing the hole-doping of the channel. We note that the formation of defects at the SiO_2/Si , corresponding to trap states below the conduction band edge, created by a 10 keV electron-beam exposure, has been reported in standard Si based MOS field-effect transistors⁷¹

Conclusions

We have studied $PdSe_2$ back gate transistors and shown that their electrical behavior can be dramatically affected by a SEM electron beam. We have highlighted that the beam has a twofold effect: it deteriorates the mobility of the $PdSe_2$ by creating intrinsic defects and changes the polarity of the device through pile-up of negative charges at the SiO_2/Si interface. The high sensitivity of $PdSe_2$ to low energy irradiation must be taken into account and can limit the use of the material in high radiation environments as well as its treatment by electron beams or plasmas. Our study suggests the opportunity to perform electrical characterization of $PdSe_2$ devices prior to SEM imaging and demonstrates the suitability of the material for low-energy radiation

detectors for medical or nuclear instrumentation as well as for environmental monitoring of caves, mines, nuclear plants or space.

Acknowledgements

We thank Shi Jun Liang from Nanjing University in China for providing the samples used in this study.

References

- (1) Choi, W.; Lahiri, I.; Seelaboyina, R.; Kang, Y. S. Synthesis of Graphene and Its Applications: A Review. *Critical Reviews in Solid State and Materials Sciences* **2010**, *35* (1), 52–71. <https://doi.org/10.1080/10408430903505036>.
- (2) Giubileo, F.; Martucciello, N.; Di Bartolomeo, A. Focus on Graphene and Related Materials. *Nanotechnology* **2017**, *28* (41), 410201. <https://doi.org/10.1088/1361-6528/aa848d>.
- (3) Manzeli, S.; Ovchinnikov, D.; Pasquier, D.; Yazyev, O. V.; Kis, A. 2D Transition Metal Dichalcogenides. *Nature Reviews Materials* **2017**, *2*, 17033.
- (4) Vogl, T.; Sripathy, K.; Sharma, A.; Reddy, P.; Sullivan, J.; Machacek, J. R.; Zhang, L.; Karouta, F.; Buchler, B. C.; Doherty, M. W.; et al. Radiation Tolerance of Two-Dimensional Material-Based Devices for Space Applications. *Nat Commun* **2019**, *10* (1), 1202. <https://doi.org/10.1038/s41467-019-09219-5>.
- (5) Bartolomeo, A. D.; Giubileo, F.; Santandrea, S.; Romeo, F.; Citro, R.; Schroeder, T.; Lupina, G. Charge Transfer and Partial Pinning at the Contacts as the Origin of a Double Dip in the Transfer Characteristics of Graphene-Based Field-Effect Transistors. *Nanotechnology* **2011**, *22* (27), 275702. <https://doi.org/10.1088/0957-4484/22/27/275702>.
- (6) Ravindra, N. M.; Tang, W.; Rassay, S. Transition Metal Dichalcogenides Properties and Applications. In *Semiconductors*; Pech-Canul, M. I., Ravindra, N. M., Eds.; Springer International Publishing: Cham, 2019; pp 333–396. https://doi.org/10.1007/978-3-030-02171-9_6.
- (7) A. D. Bartolomeo; G. Luongo; L. Lemmo; F. Urban; F. Giubileo. Graphene–Silicon Schottky Diodes for Photodetection. *IEEE Transactions on Nanotechnology* **2018**, *17* (6), 1133–1137. <https://doi.org/10.1109/TNANO.2018.2853798>.
- (8) Castro Neto, A. H.; Guinea, F.; Peres, N. M. R.; Novoselov, K. S.; Geim, A. K. The Electronic Properties of Graphene. *Rev. Mod. Phys.* **2009**, *81* (1), 109–162. <https://doi.org/10.1103/RevModPhys.81.109>.
- (9) Di Bartolomeo, A.; Pelella, A.; Liu, X.; Miao, F.; Passacantando, M.; Giubileo, F.; Grillo, A.; Lemmo, L.; Urban, F.; Liang, S. Pressure-Tunable Ambipolar Conduction and Hysteresis in Thin Palladium Diselenide Field Effect Transistors. *Adv. Funct. Mater.* **2019**, *29* (29), 1902483. <https://doi.org/10.1002/adfm.201902483>.
- (10) Xu, S.; Wu, Z.; Lu, H.; Han, Y.; Long, G.; Chen, X.; Han, T.; Ye, W.; Wu, Y.; Lin, J.; et al. Universal Low-Temperature Ohmic Contacts for Quantum Transport in Transition Metal Dichalcogenides. *2D Mater.* **2016**, *3* (2), 021007. <https://doi.org/10.1088/2053-1583/3/2/021007>.
- (11) Illarionov, Yu. Yu.; Molina-Mendoza, A. J.; Wlatl, M.; Knobloch, T.; Furchi, M. M.; Mueller, T.; Grasser, T. Reliability of Next-Generation Field-Effect Transistors with Transition Metal Dichalcogenides. In *2018 IEEE International Reliability Physics Symposium (IRPS)*; IEEE: Burlingame, CA, 2018; pp 5A.5-1-5A.5-6. <https://doi.org/10.1109/IRPS.2018.8353605>.
- (12) Sorkin, V.; Pan, H.; Shi, H.; Quek, S. Y.; Zhang, Y. W. Nanoscale Transition Metal Dichalcogenides: Structures, Properties, and Applications. *Critical Reviews in Solid State and Materials Sciences* **2014**, *39* (5), 319–367. <https://doi.org/10.1080/10408436.2013.863176>.
- (13) Childres, I.; Jauregui, L. A.; Foxe, M.; Tian, J.; Jalilian, R.; Jovanovic, I.; Chen, Y. P. Effect of Electron-Beam Irradiation on Graphene Field Effect Devices. *Appl. Phys. Lett.* **2010**, *97* (17), 173109. <https://doi.org/10.1063/1.3502610>.
- (14) Giubileo, F.; Di Bartolomeo, A.; Martucciello, N.; Romeo, F.; Lemmo, L.; Romano, P.; Passacantando, M. Contact Resistance and Channel Conductance of Graphene Field-Effect Transistors under Low-Energy Electron Irradiation. *Nanomaterials* **2016**, *6* (11), 206. <https://doi.org/10.3390/nano6110206>.

- (15) Koybasi, O.; Childres, I.; Jovanovic, I.; Chen, Y. P. Graphene Field Effect Transistor as a Radiation and Photodetector; George, T., Islam, M. S., Dutta, A., Eds.; Baltimore, Maryland, USA, 2012; p 83730H. <https://doi.org/10.1117/12.919628>.
- (16) Zeng, J.; Liu, J.; Zhang, S.; Duan, J.; Zhai, P.; Yao, H.; Hu, P.; Maaz, K.; Sun, Y. Graphene Electrical Properties Modulated by Swift Heavy Ion Irradiation. *Carbon* **2019**, *154*, 244–253. <https://doi.org/10.1016/j.carbon.2019.08.006>.
- (17) Zhao, G.-Y.; Deng, H.; Tyree, N.; Guy, M.; Lisfi, A.; Peng, Q.; Yan, J.-A.; Wang, C.; Lan, Y. Recent Progress on Irradiation-Induced Defect Engineering of Two-Dimensional 2H-MoS₂ Few Layers. *Applied Sciences* **2019**, *9* (4), 678. <https://doi.org/10.3390/app9040678>.
- (18) Kim, T.-Y.; Cho, K.; Park, W.; Park, J.; Song, Y.; Hong, S.; Hong, W.-K.; Lee, T. Irradiation Effects of High-Energy Proton Beams on MoS₂ Field Effect Transistors. *ACS Nano* **2014**, *8* (3), 2774–2781. <https://doi.org/10.1021/nn4064924>.
- (19) Tang, G.; Pam, M. E.; Zhang, H.; Shu, Z.; Feng, P.; Wei, B.; Ang, L.; Yang, H. Y.; Li, M. Fast-Neutron Irradiation Effects on Monolayer MoS₂. *Appl. Phys. Express* **2019**, *12* (5), 056001. <https://doi.org/10.7567/1882-0786/ab18b5>.
- (20) Giubileo, F.; Lemmo, L.; Passacantando, M.; Urban, F.; Luongo, G.; Sun, L.; Amato, G.; Enrico, E.; Di Bartolomeo, A. Effect of Electron Irradiation on the Transport and Field Emission Properties of Few-Layer MoS₂ Field-Effect Transistors. *J. Phys. Chem. C* **2019**, *123* (2), 1454–1461. <https://doi.org/10.1021/acs.jpcc.8b09089>.
- (21) Yoshimura, A.; Lamparski, M.; Kharche, N.; Meunier, V. First-Principles Simulation of Local Response in Transition Metal Dichalcogenides under Electron Irradiation. *Nanoscale* **2018**, *10* (5), 2388–2397. <https://doi.org/10.1039/C7NR07024A>.
- (22) Kretschmer, S.; Komsa, H.-P.; Bøggild, P.; Krasheninnikov, A. V. Structural Transformations in Two-Dimensional Transition-Metal Dichalcogenide MoS₂ under an Electron Beam: Insights from First-Principles Calculations. *J. Phys. Chem. Lett.* **2017**, *8* (13), 3061–3067. <https://doi.org/10.1021/acs.jpcclett.7b01177>.
- (23) Walker, R. C.; Shi, T.; Silva, E. C.; Jovanovic, I.; Robinson, J. A. Radiation Effects on Two-Dimensional Materials: Radiation Effects on Two-Dimensional Materials. *Phys. Status Solidi A* **2016**, *213* (12), 3065–3077. <https://doi.org/10.1002/pssa.201600395>.
- (24) Komsa, H.-P.; Kotakoski, J.; Kurasch, S.; Lehtinen, O.; Kaiser, U.; Krasheninnikov, A. V. Two-Dimensional Transition Metal Dichalcogenides under Electron Irradiation: Defect Production and Doping. *Phys. Rev. Lett.* **2012**, *109* (3), 035503. <https://doi.org/10.1103/PhysRevLett.109.035503>.
- (25) Liu, X.; Xu, T.; Wu, X.; Zhang, Z.; Yu, J.; Qiu, H.; Hong, J.-H.; Jin, C.-H.; Li, J.-X.; Wang, X.-R.; et al. Top-down Fabrication of Sub-Nanometre Semiconducting Nanoribbons Derived from Molybdenum Disulfide Sheets. *Nat Commun* **2013**, *4* (1), 1776. <https://doi.org/10.1038/ncomms2803>.
- (26) Zhao, X.; Kotakoski, J.; Meyer, J. C.; Sutter, E.; Sutter, P.; Krasheninnikov, A. V.; Kaiser, U.; Zhou, W. Engineering and Modifying Two-Dimensional Materials by Electron Beams. *MRS Bull.* **2017**, *42* (09), 667–676. <https://doi.org/10.1557/mrs.2017.184>.
- (27) Gu, H. H.; Kim, B. H.; Yoon, Y. J. Photoresponsive Behavior of Electron-Beam Irradiated MoS₂ Films. *Appl. Phys. Lett.* **2018**, *113* (18), 183103. <https://doi.org/10.1063/1.5038144>.
- (28) Chuvilin, A.; Meyer, J. C.; Algara-Siller, G.; Kaiser, U. From Graphene Constrictions to Single Carbon Chains. *New J. Phys.* **2009**, *11* (8), 083019. <https://doi.org/10.1088/1367-2630/11/8/083019>.
- (29) Sommer, B.; Sonntag, J.; Ganczarczyk, A.; Braam, D.; Prinz, G.; Lorke, A.; Geller, M. Electron-Beam Induced Nano-Etching of Suspended Graphene. *Sci Rep* **2015**, *5* (1), 7781. <https://doi.org/10.1038/srep07781>.
- (30) Oyedele, A. D.; Yang, S.; Liang, L.; Poretzky, A. A.; Wang, K.; Zhang, J.; Yu, P.; Pudasaini, P. R.; Ghosh, A. W.; Liu, Z.; et al. PdSe₂: Pentagonal Two-Dimensional Layers with High Air Stability for Electronics. *J. Am. Chem. Soc.* **2017**, *139* (40), 14090–14097. <https://doi.org/10.1021/jacs.7b04865>.
- (31) Zhang, G.; Amani, M.; Chaturvedi, A.; Tan, C.; Bullock, J.; Song, X.; Kim, H.; Lien, D.-H.; Scott, M. C.; Zhang, H.; et al. Optical and Electrical Properties of Two-Dimensional Palladium Diselenide. *Appl. Phys. Lett.* **2019**, *114* (25), 253102. <https://doi.org/10.1063/1.5097825>.

- (32) Li, E.; Wang, D.; Fan, P.; Zhang, R.; Zhang, Y.-Y.; Li, G.; Mao, J.; Wang, Y.; Lin, X.; Du, S.; et al. Construction of Bilayer PdSe₂ on Epitaxial Graphene. *Nano Res.* **2018**, *11* (11), 5858–5865. <https://doi.org/10.1007/s12274-018-2090-0>.
- (33) Long, M.; Wang, Y.; Wang, P.; Zhou, X.; Xia, H.; Luo, C.; Huang, S.; Zhang, G.; Yan, H.; Fan, Z.; et al. Palladium Diselenide Long-Wavelength Infrared Photodetector with High Sensitivity and Stability. *ACS Nano* **2019**, acsnano.8b09476. <https://doi.org/10.1021/acsnano.8b09476>.
- (34) Mak, C. H.; Lin, S.; Rogée, L.; Lau, S. P. Photoresponse of Wafer-Scale Palladium Diselenide Films Prepared by Selenization Method. *J. Phys. D: Appl. Phys.* **2020**, *53* (6), 065102. <https://doi.org/10.1088/1361-6463/ab57a8>.
- (35) Chow, W. L.; Yu, P.; Liu, F.; Hong, J.; Wang, X.; Zeng, Q.; Hsu, C.-H.; Zhu, C.; Zhou, J.; Wang, X.; et al. High Mobility 2D Palladium Diselenide Field-Effect Transistors with Tunable Ambipolar Characteristics. *Adv. Mater.* **2017**, *29* (21), 1602969. <https://doi.org/10.1002/adma.201602969>.
- (36) Qin, D.; Yan, P.; Ding, G.; Ge, X.; Song, H.; Gao, G. Monolayer PdSe₂: A Promising Two-Dimensional Thermoelectric Material. *Sci Rep* **2018**, *8* (1), 2764. <https://doi.org/10.1038/s41598-018-20918-9>.
- (37) Di Bartolomeo, A.; Pelella, A.; Urban, F.; Grillo, A.; Lemmo, L.; Passacantando, M.; Liu, X.; Giubileo, F. Field Emission in Ultrathin PdSe₂ Back-Gated Transistors. *arXiv:2002.05454 [cond-mat]* **2020**.
- (38) Long, C.; Liang, Y.; Jin, H.; Huang, B.; Dai, Y. PdSe₂: Flexible Two-Dimensional Transition Metal Dichalcogenides Monolayer for Water Splitting Photocatalyst with Extremely Low Recombination Rate. *ACS Appl. Energy Mater.* **2019**, *2* (1), 513–520. <https://doi.org/10.1021/acsaem.8b01521>.
- (39) Lin, J.; Zuluaga, S.; Yu, P.; Liu, Z.; Pantelides, S. T.; Suenaga, K. Novel Pd_2Se_3 Two-Dimensional Phase Driven by Interlayer Fusion in Layered PdSe_2 . *Phys. Rev. Lett.* **2017**, *119* (1), 016101. <https://doi.org/10.1103/PhysRevLett.119.016101>.
- (40) Fu, M.; Liang, L.; Zou, Q.; Nguyen, G. D.; Xiao, K.; Li, A.-P.; Kang, J.; Wu, Z.; Gai, Z. Defects in Highly Anisotropic Transition-Metal Dichalcogenide PdSe₂. *J. Phys. Chem. Lett.* **2019**, acs.jpcclett.9b03312. <https://doi.org/10.1021/acs.jpcclett.9b03312>.
- (41) Kempt, R.; Kuc, A.; Heine, T. *Two-Dimensional Noble-Metal Dichalcogenides and Phosphochalcogenides*; preprint; 2019. <https://doi.org/10.26434/chemrxiv.10693025.v1>.
- (42) Di Bartolomeo, A.; Pelella, A.; Liu, X.; Miao, F.; Passacantando, M.; Giubileo, F.; Grillo, A.; Lemmo, L.; Urban, F.; Liang, S. Pressure-Tunable Ambipolar Conduction and Hysteresis in Thin Palladium Diselenide Field Effect Transistors. *Adv. Funct. Mater.* **2019**, *29* (29), 1902483. <https://doi.org/10.1002/adfm.201902483>.
- (43) Giubileo, F.; Grillo, A.; Lemmo, L.; Luongo, G.; Urban, F.; Passacantando, M.; Di Bartolomeo, A. Environmental Effects on Transport Properties of PdSe₂ Field Effect Transistors. *Materials Today: Proceedings* **2020**, *20*, 50–53. <https://doi.org/10.1016/j.matpr.2019.08.226>.
- (44) Di Bartolomeo, A. Graphene Schottky Diodes: An Experimental Review of the Rectifying Graphene/Semiconductor Heterojunction. *Physics Reports* **2016**, *606*, 1–58. <https://doi.org/10.1016/j.physrep.2015.10.003>.
- (45) Di Bartolomeo, A.; Grillo, A.; Urban, F.; Lemmo, L.; Giubileo, F.; Luongo, G.; Amato, G.; Croin, L.; Sun, L.; Liang, S.-J.; et al. Asymmetric Schottky Contacts in Bilayer MoS₂ Field Effect Transistors. *Advanced Functional Materials* **2018**, *28* (28), 1800657. <https://doi.org/10.1002/adfm.201800657>.
- (46) Di Bartolomeo, A.; Giubileo, F.; Grillo, A.; Luongo, G.; Lemmo, L.; Urban, F.; Lozzi, L.; Capista, D.; Nardone, M.; Passacantando, M. Bias Tunable Photocurrent in Metal-Insulator-Semiconductor Heterostructures with Photoresponse Enhanced by Carbon Nanotubes. *Nanomaterials* **2019**, *9* (11), 1598. <https://doi.org/10.3390/nano9111598>.
- (47) Zeng, L.-H.; Wu, D.; Lin, S.-H.; Xie, C.; Yuan, H.-Y.; Lu, W.; Lau, S. P.; Chai, Y.; Luo, L.-B.; Li, Z.-J.; et al. Controlled Synthesis of 2D Palladium Diselenide for Sensitive Photodetector Applications. *Adv. Funct. Mater.* **2019**, *29* (1), 1806878. <https://doi.org/10.1002/adfm.201806878>.
- (48) Hoffman, A. N.; Gu, Y.; Liang, L.; Fowlkes, J. D.; Xiao, K.; Rack, P. D. Exploring the Air Stability of PdSe₂ via Electrical Transport Measurements and Defect Calculations. *npj 2D Mater Appl* **2019**, *3* (1), 50. <https://doi.org/10.1038/s41699-019-0132-4>.

- (49) Nguyen, G. D.; Liang, L.; Zou, Q.; Fu, M.; Oyedele, A. D.; Sumpter, B. G.; Liu, Z.; Gai, Z.; Xiao, K.; Li, A.-P. 3D Imaging and Manipulation of Subsurface Selenium Vacancies in PdSe_2 . *Phys. Rev. Lett.* **2018**, *121* (8), 086101. <https://doi.org/10.1103/PhysRevLett.121.086101>.
- (50) Kaushik, N.; Mackenzie, D. M. A.; Thakar, K.; Goyal, N.; Mukherjee, B.; Boggild, P.; Petersen, D. H.; Lodha, S. Reversible Hysteresis Inversion in MoS_2 Field Effect Transistors. *npj 2D Mater Appl* **2017**, *1* (1), 34. <https://doi.org/10.1038/s41699-017-0038-y>.
- (51) Di Bartolomeo, A.; Genovese, L.; Giubileo, F.; Lemmo, L.; Luongo, G.; Foller, T.; Schleberger, M. Hysteresis in the Transfer Characteristics of MoS_2 Transistors. *2D Mater.* **2017**, *5* (1), 015014. <https://doi.org/10.1088/2053-1583/aa91a7>.
- (52) Urban, F.; Martucciello, N.; Peters, L.; McEvoy, N.; Di Bartolomeo, A. Environmental Effects on the Electrical Characteristics of Back-Gated WSe_2 Field-Effect Transistors. *Nanomaterials* **2018**, *8* (11), 901. <https://doi.org/10.3390/nano8110901>.
- (53) Gu, D.; Dey, S. K.; Majhi, P. Effective Work Function of Pt, Pd, and Re on Atomic Layer Deposited HfO_2 . *Appl. Phys. Lett.* **2006**, *89* (8), 082907. <https://doi.org/10.1063/1.2336718>.
- (54) Tsai, C.-H.; Chen, K.-J.; Pan, F.-M.; Lo, H.-Y.; Li, Y.; Chiang, M.-C.; Mo, C.-N. Effects of Hydrogen Plasma Treatment on Field-Emission Characteristics of Palladium Nanogap Emitters. *J. Electrochem. Soc.* **2008**, *155* (12), J361. <https://doi.org/10.1149/1.2988646>.
- (55) Urban, F.; Martucciello, N.; Peters, L.; McEvoy, N.; Di Bartolomeo, A. Environmental Effects on the Electrical Characteristics of Back-Gated WSe_2 Field-Effect Transistors. *Nanomaterials* **2018**, *8* (11), 901. <https://doi.org/10.3390/nano8110901>.
- (56) Zou, D.; Yu, C.; Li, Y.; Ou, Y.; Gao, Y. Pressure-Induced Enhancement in the Thermoelectric Properties of Monolayer and Bilayer SnSe_2 . *R. Soc. open sci.* **2018**, *5* (3), 171827. <https://doi.org/10.1098/rsos.171827>.
- (57) Lemmo, L.; Urban, F.; Giubileo, F.; Passacantando, M.; Di Bartolomeo, A. Nanotip Contacts for Electric Transport and Field Emission Characterization of Ultrathin MoS_2 Flakes. *Nanomaterials* **2020**, *10* (1), 106. <https://doi.org/10.3390/nano10010106>.
- (58) Di Bartolomeo, A.; Urban, F.; Passacantando, M.; McEvoy, N.; Peters, L.; Lemmo, L.; Luongo, G.; Romeo, F.; Giubileo, F. A WSe_2 Vertical Field Emission Transistor. *Nanoscale* **2019**, *11* (4), 1538–1548. <https://doi.org/10.1039/C8NR09068H>.
- (59) Giubileo, F.; Di Bartolomeo, A. The Role of Contact Resistance in Graphene Field-Effect Devices. *Progress in Surface Science* **2017**, *92* (3), 143–175. <https://doi.org/10.1016/j.progsurf.2017.05.002>.
- (60) Bartolomeo, A. D.; Giubileo, F.; Romeo, F.; Sabatino, P.; Carapella, G.; Lemmo, L.; Schroeder, T.; Lupina, G. Graphene Field Effect Transistors with Niobium Contacts and Asymmetric Transfer Characteristics. *Nanotechnology* **2015**, *26* (47), 475202. <https://doi.org/10.1088/0957-4484/26/47/475202>.
- (61) Liang, Q.; Wang, Q.; Zhang, Q.; Wei, J.; Lim, S. X.; Zhu, R.; Hu, J.; Wei, W.; Lee, C.; Sow, C.; et al. High-Performance, Room Temperature, Ultra-Broadband Photodetectors Based on Air-Stable PdSe_2 . *Adv. Mater.* **2019**, 1807609. <https://doi.org/10.1002/adma.201807609>.
- (62) Yang, M.; Kim, T.-Y.; Lee, T.; Hong, S. Nanoscale Enhancement of Photoconductivity by Localized Charge Traps in the Grain Structures of Monolayer MoS_2 . *Sci Rep* **2018**, *8* (1), 15822. <https://doi.org/10.1038/s41598-018-34209-w>.
- (63) Du, Y.; Liu, H.; Neal, A. T.; Si, M.; Ye, P. D. Molecular Doping of Multilayer MoS_2 Field-Effect Transistors: Reduction in Sheet and Contact Resistances. *IEEE Electron Device Lett.* **2013**, *34* (10), 1328–1330. <https://doi.org/10.1109/LED.2013.2277311>.
- (64) Matsuoka, H.; Kanahashi, K.; Tanaka, N.; Shoji, Y.; Li, L.-J.; Pu, J.; Ito, H.; Ohta, H.; Fukushima, T.; Takenobu, T. Chemical Hole Doping into Large-Area Transition Metal Dichalcogenide Monolayers Using Boron-Based Oxidant. *Jpn. J. Appl. Phys.* **2018**, *57* (2S2), 02CB15. <https://doi.org/10.7567/JJAP.57.02CB15>.
- (65) Drouin, D.; Couture, A. R.; Joly, D.; Tastet, X.; Aimez, V.; Gauvin, R. CASINO V2.42—A Fast and Easy-to-Use Modeling Tool for Scanning Electron Microscopy and Microanalysis Users. *Scanning* **2007**, *29* (3), 92–101. <https://doi.org/10.1002/sca.20000>.

- (66) Demers, H.; Poirier-Demers, N.; Couture, A. R.; Joly, D.; Guilmain, M.; de Jonge, N.; Drouin, D. Three-Dimensional Electron Microscopy Simulation with the CASINO Monte Carlo Software. *Scanning* **2011**, *33* (3), 135–146. <https://doi.org/10.1002/sca.20262>.
- (67) Komsa, H.-P.; Kurasch, S.; Lehtinen, O.; Kaiser, U.; Krashennikov, A. V. From Point to Extended Defects in Two-Dimensional MoS₂: Evolution of Atomic Structure under Electron Irradiation. *Phys. Rev. B* **2013**, *88* (3), 035301. <https://doi.org/10.1103/PhysRevB.88.035301>.
- (68) Chen, T.-Y.; Pang, C.-S.; Hwu, J.-G. Effect of Electrons Trapping/De-Trapping at Si-SiO₂ Interface on Two-State Current in MOS(p) Structure with Ultra-Thin SiO₂ by Anodization. *ECS J. Solid State Sci. Technol.* **2013**, *2* (9), Q159–Q164. <https://doi.org/10.1149/2.025309jss>.
- (69) Shamir, N.; Mihaychuk, J. G.; van Driel, H. M. Trapping and Detrapping of Electrons Photoinjected from Silicon to Ultrathin SiO₂ Overlayers. I. In Vacuum and in the Presence of Ambient Oxygen. *Journal of Applied Physics* **2000**, *88* (2), 896–908. <https://doi.org/10.1063/1.373753>.
- (70) Di Bartolomeo, A.; Rücker, H.; Schley, P.; Fox, A.; Lischke, S.; Na, K.-Y. A Single-Poly EEPROM Cell for Embedded Memory Applications. *Solid-State Electronics* **2009**, *53* (6), 644–648. <https://doi.org/10.1016/j.sse.2009.04.007>.
- (71) Kim, J.-S.; Tyryshkin, A. M.; Lyon, S. A. Annealing Shallow Si/SiO₂ Interface Traps in Electron-Beam Irradiated High-Mobility Metal-Oxide-Silicon Transistors. *Appl. Phys. Lett.* **2017**, *110* (12), 123505. <https://doi.org/10.1063/1.4979035>.